ISSN (Print) 1226-1750
ISSN (Online) 2233-6656
Journal of Magnetics 28(1), 16-23 (2023) https://doi.org/10.4283/JMAG.2023.28.1.016

Investigation of Slip Conditions and Magnetic Force on Generalized 3D Flow with Heat Transfer Phenomenon Due To Lower Unbend Wall Channel

Tasawar Abbas[1]*, Kaouther Ghachem[2], Sami Ullah Khan[3], Bilal Ahmad[1], Muapper Alhadri[4], and Lioua Kolsi[4,5]

[1]*Department of Mathematics, University of Wah, Wah Cantt, 47040 Pakistan*
[2]*Department of Industrial Engineering and Systems, College of Engineering, Princess Nourah bint Abdulrahman University, P.O. Box 84428, Riyadh 11671, Saudi Arabia*
[3]*Department of Mathematics, Namal University, Mianwali 42250, Pakistan*
[4]*Department of Mechanical Engineering, College of Engineering, University of Ha'il, Ha'il City, Saudi Arabia*
[5]*Laboratory of Metrology and Energy Systems, National Engineering School, Energy Engineering Department, University of Monastir, 5000 Monastir, Tunisia*

(Received 21 September 2021, Received in final form 7 March 2023, Accepted 8 March 2023)

The fluid flow under the slip effects present many dynamical applications in petroleum engineering, soil sciences, aerodynamics, thermal systems etc. The aim of current investigation is to observe the heat transfer phenomenon in magnetized flow of viscous fluid due channel with lower unbend wall. The fluid flow is altered due to interaction of slip effects. The injection phenomenon for porous medium has been considered. For heat transfer investigation, viscous dissipation applications are endorsed. The fundamental problem is modelled with associated laws. The variational iteration method (VIM) scheme is proposed to simulate the analytical outcomes. The numerical results for Nusselt number and skin friction coefficient are depicted and analysed graphically. The summarized observations convey that control of heat transfer is improved with interaction of slip phenomenon. The declining result for Nusselt number is referred to suction parameter.

Keywords : MHD flow, velocity slip, temperature jump, variational iteration method (VIM)

1. Introduction

The flow and transfer of heat over stretching/shrinking surfaces have large application in the field of production procedure of artificial fibres and artificial film, metallic sheets cooling in baths and aerodynamics extrusion processes. Sakiadis [1] presented first two dimensional problem for moving surfaces. Crane [2] obtained closed form solution for viscous fluid flow due to stretching surface. Lakshmisha *et al.* [3] extended the analysis of Crane [2] for three dimensional case. The series solution simulations for heat transfer problem against the impulsively stretching plate was examined by Guled *et al.* [4]. The study of mass transfer for MHD flow with porous space was performed by Hayat *et al.* [5]. Barkakoti and Bharali [6] analyzed the fluid interaction for channel flow with deviation of lower surface. Majeed *et al.* [7] determined the heat transfer prediction for velocity slip flow with tiny particles. The multiple slip effects with heat transfer prediction via stretched geometry was focused by Majeed *et al.* [8]. Jawad *et al.* [9] explained the heating impact of bio-nanoparticles with Nield convective approach. Majeed *et al.* [10] endorsed the heat fluctuation for Casson material with nonlinearly stretched surface.

In fluid mechanics, the boundary layer is the well-known concepts for fluid flow due to solid surfaces. Usually, the no-slip boundary condition is valid for macroscopic flows [11]. Navier [12] claimed that the slip shear stress is proportional to quantity of liquid at the solid surface. Akyildiz *et al.* [13] suggested that the slip length is directly proportional to velocity component. Wang [14] introduced the surface suction and slip velocity consequences for moving surface flows. Hayat *et al.* [15] deduced the observations for slip phenomenon for porous channel geometry.

Current research endorsed the heat transfer phenomenon

*Corresponding author: Tel: +92-51-9157000
e-mail: tasawar.abbas@uow.edu.pk

regarding the viscous fluid flow due to lower unbend channel under the influence of slip effects. The fluid flow is subject to injection framework. The assessment of heat transfer is reported under the contribution of joule heating. The convective thermal constraints are utilized to assess the heat transfer impact. The analytical outcomes of problem are simulated via variational iteration method [16-20]. Current results report applications in plasma physics, thermal engineering, aerodynamics, extrusion systems, manufacturing processes etc.

2. Mathematical Formulation

Let consider an electrically conducting incompressible steady flow of viscous fluid due to parallel plates separated at distance h. The upper plate ($z = h$) is porous while the base plate is stretched in both directions with different rates comprising the constant injection. The magnetic field with constant magnitude is implemented along z-axis. No contribution of electric force is being considered. The induced magnetic field is neglected under the small Reynolds number consideration. The lower plate is sustained at constant temperature T_w while T_0 is the fluid temperature. Additionally, Joule heating and viscous dissipation features are considered. The governing equations are.

$$\nabla \cdot \mathbf{V} = 0, \tag{1}$$

$$\frac{d\mathbf{V}}{dt} = -\frac{1}{\rho}(\nabla p - \mu \nabla^2 \mathbf{V} - \mathbf{J} \times \mathbf{B}), \tag{2}$$

$$c_p \frac{dT}{dt} = \frac{1}{\rho}(k\nabla^2 T + \mu \,\mathrm{tr}(\mathbf{AL}) + \frac{1}{\sigma}\mathbf{J} \cdot \mathbf{J}), \tag{3}$$

where gradient operator is ∇, p is pressure, material derivative is denoted with d/dt, μ is dynamic viscosity, ρ is fluid density, electrical conductivity is expressed with σ, k is thermal conductivity while c_p is constant pressure. Defining **J** and **A** as:

$$\mathbf{J} = \sigma(\mathbf{V} \times \mathbf{B}), \tag{4}$$

$$\mathbf{A} = \mathbf{L} + \mathbf{L}^{\mathrm{T}}. \tag{5}$$

Here $\mathbf{L}^{\mathrm{T}}$ shows the transpose of **L**. The temperature and velocity fields are considered as:

$$T = T(x, y, z), \mathbf{V} = \big(u(x, y, z), v(x, y, z), w(x, y, z)\big),$$

The velocity components are u, v and w are taken along x, y and z axes, respectively. Under such assumptions, the governing equations are:

$$\frac{\partial u}{\partial x} + \frac{\partial v}{\partial y} + \frac{\partial w}{\partial z} = 0, \tag{6}$$

$$u\frac{\partial u}{\partial x} + v\frac{\partial u}{\partial y} + w\frac{\partial u}{\partial z} = -\frac{1}{\rho}\frac{\partial p}{\partial x} + \upsilon\left(\frac{\partial^2 u}{\partial x^2} + \frac{\partial^2 u}{\partial y^2} + \frac{\partial^2 u}{\partial z^2}\right) - \frac{\sigma B_0^2}{\rho}u, \tag{7}$$

$$u\frac{\partial v}{\partial x} + v\frac{\partial v}{\partial y} + w\frac{\partial v}{\partial z} = -\frac{1}{\rho}\frac{\partial p}{\partial y} + \upsilon\left(\frac{\partial^2 v}{\partial x^2} + \frac{\partial^2 v}{\partial y^2} + \frac{\partial^2 v}{\partial z^2}\right) - \frac{\sigma B_0^2}{\rho}v, \tag{8}$$

$$u\frac{\partial w}{\partial x} + v\frac{\partial w}{\partial y} + w\frac{\partial w}{\partial z} = -\frac{1}{\rho}\frac{\partial p}{\partial z} + \upsilon\left(\frac{\partial^2 w}{\partial x^2} + \frac{\partial^2 w}{\partial y^2} + \frac{\partial^2 w}{\partial z^2}\right), \tag{9}$$

$$u\frac{\partial T}{\partial x} + v\frac{\partial T}{\partial y} + w\frac{\partial T}{\partial z} = \frac{k}{\rho c_p}\left(\frac{\partial^2 T}{\partial x^2} + \frac{\partial^2 T}{\partial y^2} + \frac{\partial^2 T}{\partial z^2}\right) + \frac{\sigma B_0^2}{\rho c_p}(u^2 + v^2) + \frac{\upsilon}{c_p}\left(2\left(\frac{\partial u}{\partial x}\right)^2 + 2\left(\frac{\partial v}{\partial y}\right)^2 + 2\left(\frac{\partial w}{\partial z}\right)^2 + \left(\frac{\partial u}{\partial y} + \frac{\partial v}{\partial x}\right)^2 + \left(\frac{\partial u}{\partial z} + \frac{\partial w}{\partial x}\right)^2 + \left(\frac{\partial v}{\partial z} + \frac{\partial w}{\partial y}\right)^2\right). \tag{10}$$

The appropriate boundary conditions are:

$$\begin{gathered} u - \beta_1\left(\frac{\partial u}{\partial z} + \frac{\partial w}{\partial x}\right) = ax, \quad v - \beta_1\left(\frac{\partial v}{\partial z} + \frac{\partial w}{\partial y}\right) = by, \quad w = 0, \\ T - \gamma_1\frac{\partial T}{\partial z} = T_w, \quad \text{at } z = 0, \\ u + \beta_1\left(\frac{\partial u}{\partial z} + \frac{\partial w}{\partial x}\right) = 0, \quad v + \beta_1\left(\frac{\partial v}{\partial z} + \frac{\partial w}{\partial y}\right) = 0, \quad w = -v_0, \\ T + \gamma_1\frac{\partial T}{\partial z} = T_0, \quad \text{at } z = h, \end{gathered} \tag{11}$$

where $\upsilon = \mu/\rho$ is the kinematic viscosity, v_0 is constant injection velocity is at upper plate, γ_1 be thermal slip parameter and β_1 velocity slip parameter.

The similarity transformations are [8].

$$\begin{gathered} T = (T_w - T_0)\theta(\eta) + T_0, \; v = yag'(\eta), \eta = \frac{z}{h}, \\ w = -ah\big(f(\eta) + g(\eta)\big), u = xaf'(\eta). \end{gathered} \tag{12}$$

The continuity equation (6) is satisfied by virtue of the above transformations while equations (7-11) reduce to following form:

$$f'''' - M^2 f'' - \mathrm{Re}(f'f'' - gf''' - g'f'' - ff''') = 0, \tag{13}$$

$$g'''' - M^2 g'' - \mathrm{Re}(g'g'' - gg''' - f'g'' - fg''') = 0, \tag{14}$$

$$\theta'' + \mathrm{Pr}\begin{pmatrix} 4\,\mathrm{Re}\,\mathrm{Ec}(f'^2 + f'g' + g'^2) + \mathrm{Ec}_y(M^2 g'^2 + g''^2) \\ + \mathrm{Re}(f + g)\theta' + \mathrm{Ec}_x(f''^2 + M^2 f'^2) \end{pmatrix} = 0, \tag{15}$$

$$\begin{gathered} f'(0) - \beta f''(0) = 1, \quad g'(0) - \beta g''(0) = c, \\ f(0) + g(0) = 0, \quad \theta(0) - \gamma\theta'(0) = 1, \\ f'(1) + \beta f''(1) = 0, \quad g'(1) + \beta g''(1) = 0, \\ f(1) + g(1) = V_0, \quad \theta(1) + \gamma\theta'(1) = 0, \end{gathered} \tag{16}$$

with Reynolds number Re, Hartmann number M, Prandtl number Pr, stretching ratio parameter c, dimensionless velocity parameter β, thermal slip parameters γ, injection parameter V_0, Ec_x be local Eckert number along x direction while Ec_y be Eckert number along y direction. Defining these parameters as:

$$\mathrm{Re}=\frac{ah^2}{\upsilon},\quad M^2=\frac{\alpha B_0^2 h^2}{\mu},\quad \mathrm{Pr}=\frac{\mu c_p}{k},\quad c=\frac{b}{a},$$
$$\beta=\frac{\beta_1}{h},\quad \gamma=\frac{\gamma_1}{h},\quad V_0=\frac{v_0}{ah},\quad Ec=\frac{a\upsilon}{c_p(T_w-T_0)},$$
$$Ec_x=\frac{a^2x^2}{c_p(T_w-T_0)},\quad Ec_y=\frac{a^2y^2}{c_p(T_w-T_0)}.$$

The interesting physical quantities are Nusselt number and skin friction coefficient with relations:

$$C_{fx}=-\frac{\mu}{\rho(ax)^2}\left(\frac{\partial u}{\partial z}+\frac{\partial w}{\partial y}\right)_{z=0},\ C_{fy}=-\frac{\mu}{\rho(ay)^2}\left(\frac{\partial v}{\partial z}+\frac{\partial w}{\partial x}\right)_{z=0},$$
$$Nu=-\frac{k(\partial T/\partial z)_{z=0}}{k(T_w-T_0)}. \tag{17}$$

Using transformation (12), dimensionless form of expression (17) is:

$$\mathrm{Re}^{1/2}\mathrm{Re}_x^{1/2}C_{fx}=-f''(0),\ \mathrm{Re}^{1/2}\mathrm{Re}_y^{1/2}C_{fy}=-g''(0),\ Nu=-\theta'(0), \tag{18}$$

where $\mathrm{Re}_x=ax^2/\upsilon$ and $\mathrm{Re}_y=ay^2/\upsilon$ are the local Reynolds numbers.

3. Variational Iteration Method

There are several analytical techniques are available in existing knowledge. The variational iteration method (VIM) identifies its novelty and soundness due to its higher accuracy. The simulations for many nonlinear problems can be easily computed by using VIM successfully.

The general form differential equation is:

$$Lv+Nv=g(x), \tag{19}$$

Justified correction expressions are:

$$v_{n+1}=v_n(x)+\int_0^x\lambda(t)\left[Lv_n(t)+Nv_n(t)-g(t)\right]dt, \tag{20}$$

where

$$v(x)=\lim_{n\to\infty}v_n(x). \tag{21}$$

3.1. Solution procedure with VIM

The bases expressions are:

$$\{\eta^n;n\geq 0\}, \tag{22}$$

In the form

$$f(\eta)=\sum_{n=1}^{\infty}a_n\eta^n,g(\eta)=\sum_{n=1}^{\infty}b_n\eta^n,\theta(\eta)=c_0+\sum_{n=1}^{\infty}c_n\eta^n, \tag{23}$$

$$f_0(\eta)=\frac{(1+2\beta)(1+3V_0\beta)+2\beta}{(1+2\beta)(1+6\beta)}\eta+\frac{(1+2\beta)(3V_0-4)-4\beta}{2(1+2\beta)(1+6\beta)}\eta^2+\frac{(1-V_0)}{(1+6\beta)}\eta^3, \tag{24}$$

$$g_0(\eta)=\frac{(1+2\beta)(c+3V_0\beta)+2\beta c}{(1+2\beta)(1+6\beta)}\eta+\frac{(1+2\beta)(3V_0-4c)-4\beta c}{2(1+2\beta)(1+6\beta)}\eta^2+\frac{(c-V_0)}{(1+6\beta)}\eta^3, \tag{25}$$

$$\theta_0(\eta)=\frac{1}{1+2\gamma}(1+\gamma-\eta), \tag{26}$$

Defining correction functions:

$$f_{n+1}(\eta)=f_n(\eta)+\int_0^\eta\lambda_f(s)[f_n''''-\mathrm{Re}(f_n'f_n''-f_nf_n'''-g_nf_n'''-g_n'f_n'')-M^2f_n'']ds, \tag{27}$$

$$g_{n+1}(\eta)=g_n(\eta)+\int_0^\eta\lambda_g(s)[g_n''''-\mathrm{Re}(g_n'g_n''-f_ng_n'''-g_ng_n'''-f_n'g_n'')-M^2g_n'']ds, \tag{28}$$

$$\theta_{n+1}(\eta)=\theta_n(\eta)+\int_0^\eta\lambda_\theta(s)[\theta_n''+\mathrm{Pr}\begin{pmatrix}\mathrm{Re}(f_n+g_n)\theta_n'+4\,\mathrm{Re}\,\mathrm{Ec}(f_n'^2+g_n'^2+f_n'g_n')+\\ \mathrm{Ec}_x(f_n''^2+M^2f_n'^2)+\mathrm{Ec}_y(g_n''^2+M^2g_n'^2)\end{pmatrix}]ds, \tag{29}$$

$$\lambda_f(s)=\frac{-(\eta-s)^3}{3!},\ \lambda_g(s)=\frac{-(\eta-s)^3}{3!},\ \lambda_\theta(s)=(\eta-s) \tag{30}$$

The final solution of the above equation is:

$$f(\eta)=\lim_{n\to\infty}f_{n+1}(\eta)$$
$$g(\eta)=\lim_{n\to\infty}g_{n+1}(\eta) \tag{31}$$
$$\theta(\eta)=\lim_{n\to\infty}\theta_{n+1}(\eta)$$

Table 1. Convergence of VIM result for numerous Iterations when $\mathrm{Re}=M=V_0=1.0$, $\beta=0.1=\gamma$, $c=0.5=\mathrm{Pr}=\mathrm{Ec}=\mathrm{Ec}_x=\mathrm{Ec}_y$, $\hbar_1=-0.9=\hbar_2$ and $\hbar_3=-1$.

Iterations	$-f''(0)$	$g''(0)$	$-\theta'(0)$
1	0.8854166667	0.5650038946	0.1673583984
2	0.8886368797	0.5679240872	0.1689020499
5	0.8887364916	0.5680176836	0.1688332916
9	0.8887365708	0.5680177467	0.1688334106
10	0.8887365708	0.5680177467	0.1688334106
15	0.8887365708	0.5680177467	0.1688334106
20	0.8887365708	0.5680177467	0.1688334106
40	0.8887365708	0.5680177467	0.1688334106
50	0.8887365708	0.5680177467	0.1688334106

The software Maple-18 is used to solve the system of equations (24)-(30). The accuracy of results via current method is proposed in Table 1. A fine accuracy of results is obtained upon increasing the iterations,.

4. Physical Analysis

The physical outcomes of problem are observed in this section. The numerical solution is computed for shooting method. The convincing comparative reflection of results is observed as shown in Fig. 1. Physical investigation for parameters is reported for velocity, temperature and shear stress coefficient. Figs. (2-9) are prepared in order to examine the effects of Hartmann number M and slip parameter β on velocity components ($f'(\eta)$, $g'(\eta)$, $f(\eta)$, $g(\eta)$). Fig. 2 indicates that with increasing the magnitude of β, f' decline in the lower part of channel while opposite trend is observed in top half channel surface. Such observations are confirmed the analysis of Hayat *et al.* [5]. Physically with increasing slip parameter, the fluid particles experienced a retarding force due to the increase in slip length which slows down the flow. However, this decrease in the fluid velocity is recompensed in the top part of channel due to injection phenomenon. Fig. 3 presents the impact of Hartmann number M on f'. It is observed that in the first instance, f' dwindled with for$M$ for $\eta = 0.5$ and started gradually with increasing M. Such results demonstrate the Lorentz force applications. Figs. 4 and 5 demonstrate that f declined for β and M. Figs. (6-9) explain the influence of β and M on g' and g. Each of these figures is plotted for two different cases of equal and unequal stretching along both directions. It is seen that for equal stretching in both lateral directions, β and M have similar effects on g' and g like f' and f. Fig. 11 shows that for $c < 1$, the magnitude of g' increases in top and lower channel walls for larger β. To satisfy the mass conservation constraint, the fluid flow is correspondingly delayed in the mid part of the channel. The behaviour of g' for upgrading M is pronounced via Fig. 7 for equal and

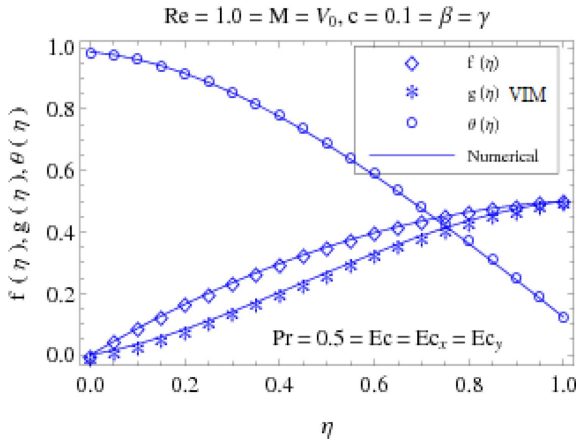

Fig. 1. (Color online) Comparison of Variational Iteration Method and numerical solutions.

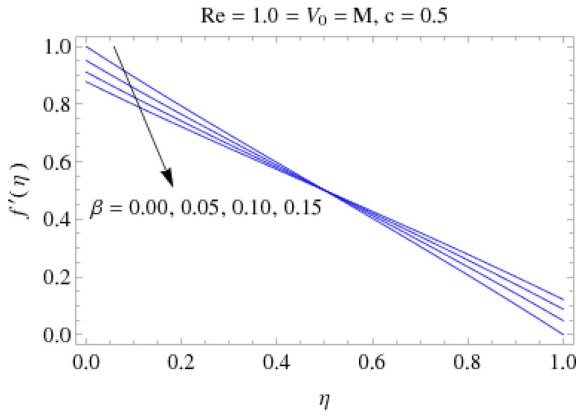

Fig. 2. (Color online) $f'(\eta)$ is Velocity profile for various values of slip parameter β.

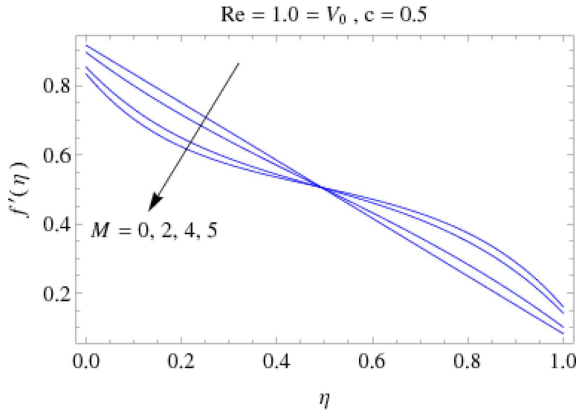

Fig. 3. (Color online) $f'(\eta)$ is Velocity profile for various values of magnetic parameter M.

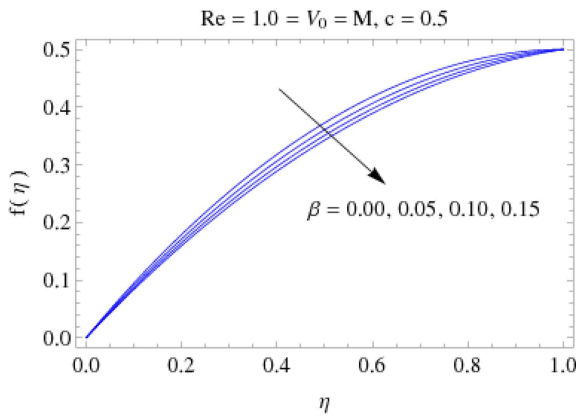

Fig. 4. (Color online) $f(\eta)$ is velocity profile for various values of slip parameter β.

unequal stretching cases. The impact of β on g is portrayed in Fig. 8. It is interesting to note that for $c < 1$, the behaviour of g is totally different as compared to $c = 1$. It raises in bottom half and decreases in remaining half regime of channel for increasing β. The variation in g with changing M is given in Fig. 9. Figs. (10-13) are devoted to show the influence of β, M and c on skin friction coefficient components $(-f''(0), -g''(0))$. The wall shear force for M and c against specific values of β

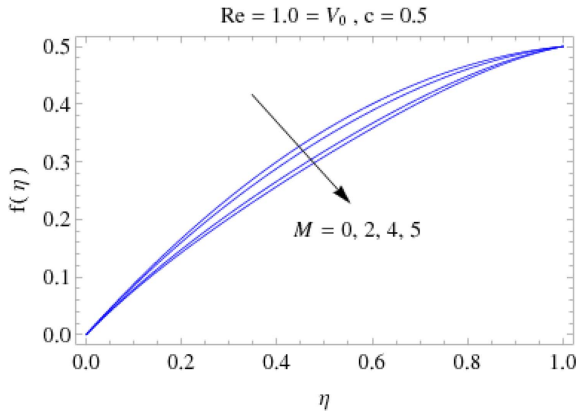

Fig. 5. (Color online) $f(\eta)$ is velocity profile for various values of magnetic parameter M.

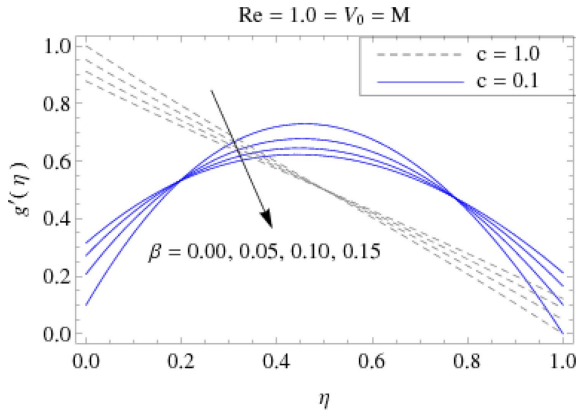

Fig. 6. (Color online) Velocity profile $g'(\eta)$ for various values of slip parameter β.

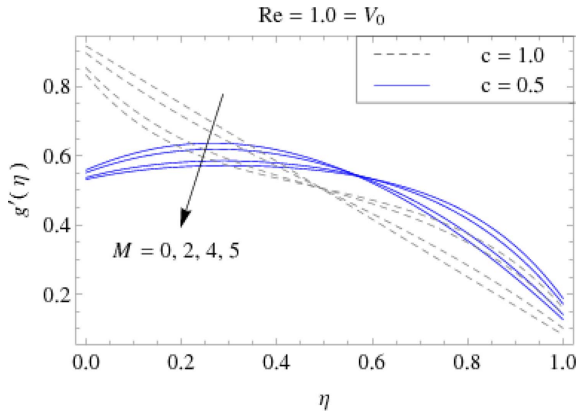

Fig. 7. (Color online) Velocity profile $g'(\eta)$ for various values of magnetic parameter M.

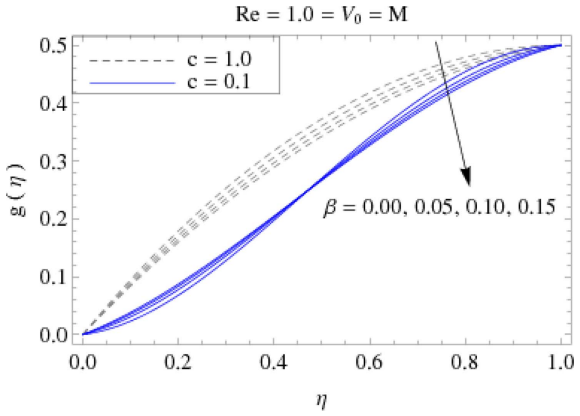

Fig. 8. (Color online) Velocity profile $g(\eta)$ for various values of slip parameter β.

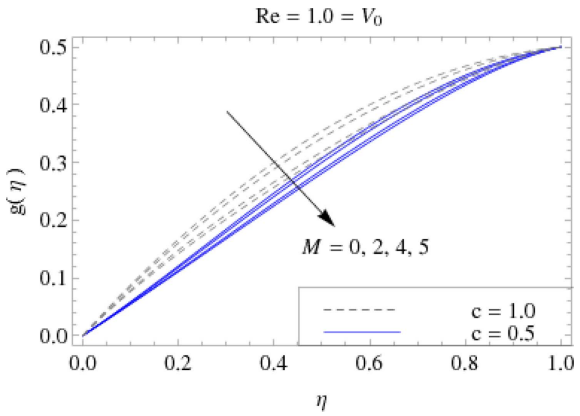

Fig. 9. (Color online) Velocity profile $g(\eta)$ for various values of magnetic parameter M.

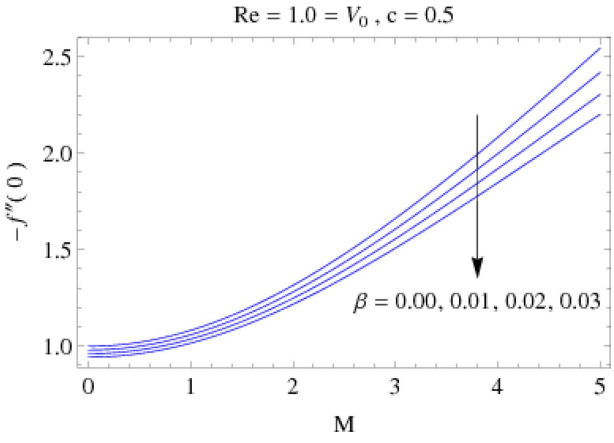

Fig. 10. (Color online) Effects of M and β on $-f''(0)$.

is noticed in Figs. 10 and 11. Fig. 10 indicates that upon enhancing β, a decrease in $-f''(0)$ is observed while opposite is examined for M. Fig. 11 demonstrates that c has negligible effects on $-f''(0)$. The coefficient of skin friction along both directions is plotted for M and β is expressed in Figs. 12 and 13, respectively. Fig. 12 illustrates that $-g''(0)$ increases with growing values of β and M. Fig. 18 shows that $-g''(0)$ rises for β when $c < 0.9$ but declined for $c > 0.9$. Figs. (14-18) are prepared in order to display the impacts of β and M on temperature and temperature gradient profiles. Fig. 14 is plotted to assess the onset of temperature field against η for in view of thermal slip parameter γ. The analysis is examined for both appearance and absence of viscous dissipation. It is analysed that with larger γ, the temperature profile reduces in the lower plate surface region while it increases in opposite plate surface region subject to the viscous dissipation effects. However, impact of γ on temperature profile near the lower plate surface region is not prominent when viscous dissipation effects are dominant. Fig. 15 demonstrates that temperature profile declines for enhancing β. In Fig. 16, it might be observed that Joule heating affects the temperature profile in presence of M. A raise in M corresponds to Joule heating effects enhanced the fluid temperature effectively. In Fig. 17, the temperature gradient $-\theta'(0)$ is plotted against M in presence of thermal slip parameter γ. In addition, it is

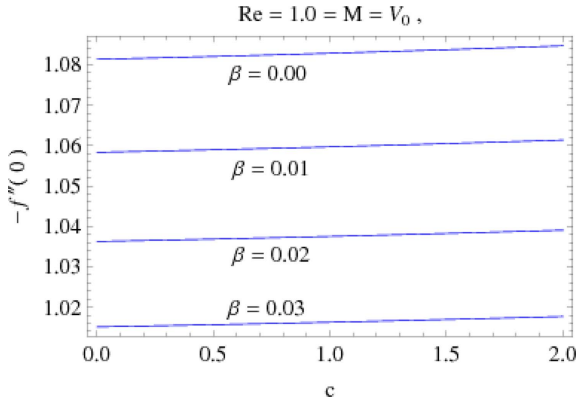

Fig. 11. (Color online) Effects of c and β on $-f''(0)$.

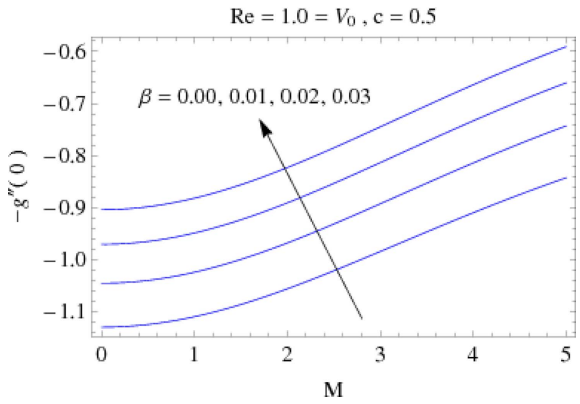

Fig. 12. (Color online) Effects of M and β on $-g''(0)$.

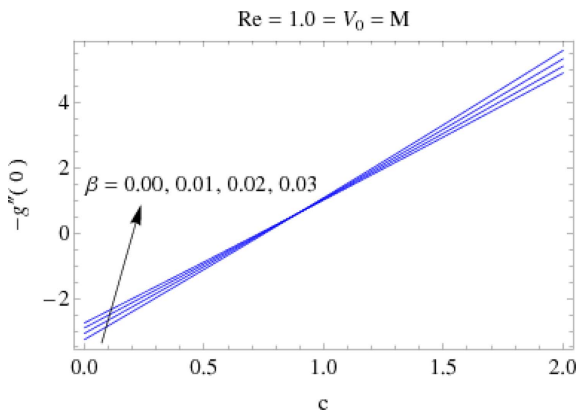

Fig. 13. (Color online) Effects of parameters c and β on $-g''(0)$.

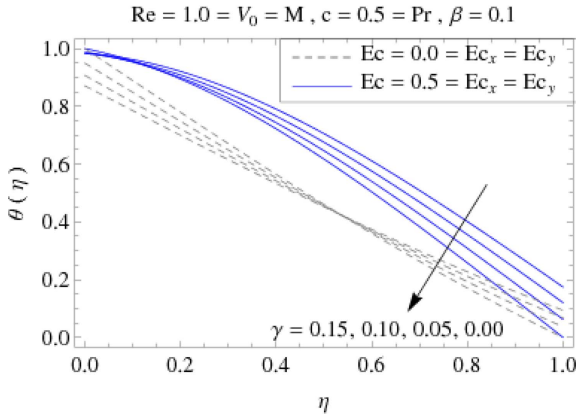

Fig. 14. (Color online) Temperature profile $\theta(\eta)$ for various values of slip parameter γ.

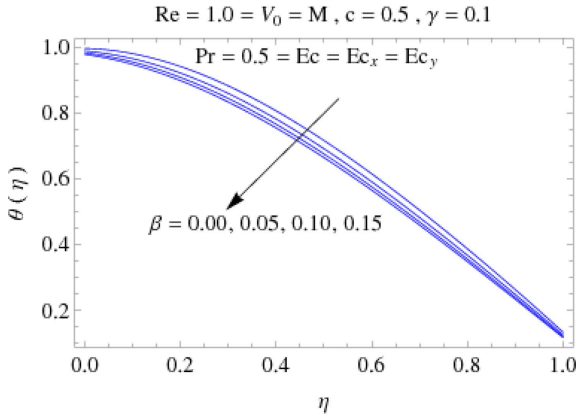

Fig. 15. (Color online) Temperature profile $\theta(\eta)$ for various values of slip parameter β.

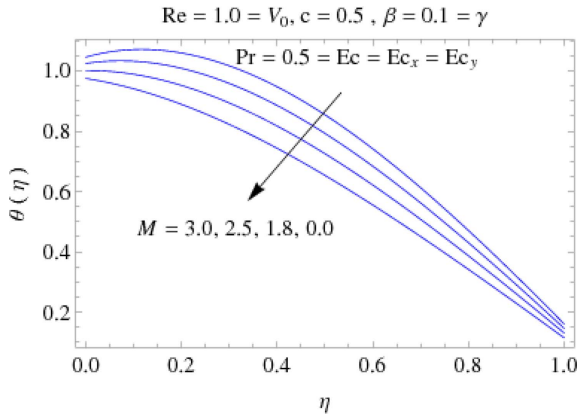

Fig. 16. (Color online) Temperature profile $\theta(\eta)$ for various values of magnetic parameter M.

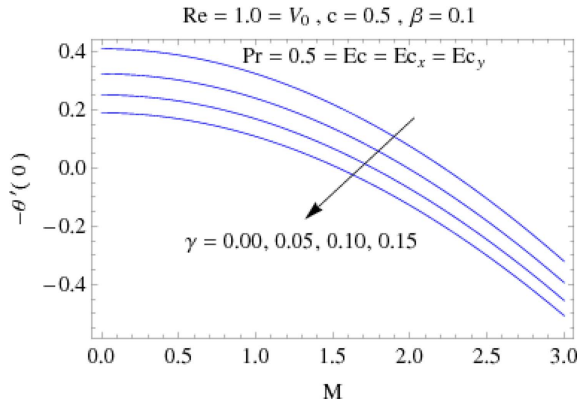

Fig. 17. (Color online) Effects of M and γ on $-\theta'(0)$.

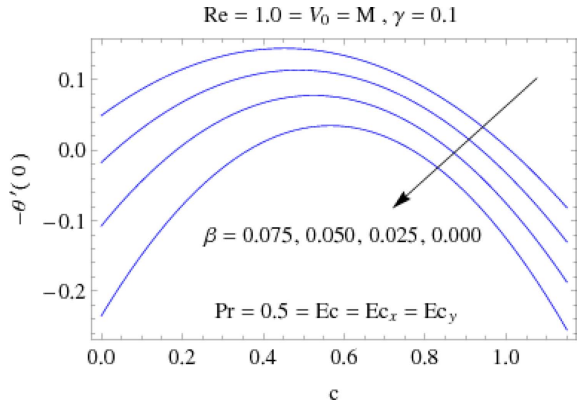

Fig. 18. (Color online) Effects of c and β on $-\theta'(0)$.

shown that rate of heat transfer decreases due to M and γ. Fig. 18 has been prepared to observe change in $-\theta'(0)$ against c in view of β. It is clearly seen that rate of heat transfer increases with increasing β. The impact of c on $-\theta'(0)$ is different and interesting. Initially, an increasing depiction for up leading c is noticed while it decreases gradually after some interval. This implies that the heat transfer rate can be maximized by for larger stretching ratio parameter.

5. Conclusion

The heat transfer assessment of viscous material with channel surface flow is prescribed under slip effects. The thermal transport of problem is noticed in view of Joule heating and convective boundary constraints. The slip features are used to analyse the flow phenomenon. The variation iteration outcomes are presented. The significant outcomes are:

- The fluctuation in velocity and thermal transport is noted due to stretching ratio parameter.
- An increasing impact of velocity parameter on wall shear force is depicted.
- A controls of temperature profile against velocity slip parameter is observed.
- The boosted thermal profile subject to magnetic parameter is claimed.
- The Nusselt number declined due to slip parameter and Hartman number.

Acknowledgement

Princess Nourah bint Abdulrahman University Researchers Supporting Project number (PNURSP2023R41), Princess Nourah bint Abdulrahman University, Riyadh, Saudi Arabia.

References

[1] B. C. Sakiadis, AIChE Journal. **7**, 26 (1961).
[2] L. J. Crane, ZAMP. **21**, 645 (1970).
[3] K. N. Lakshmisha, S. Venkateswaran, and G. Nath, J. Heat Transfer. **110**, 590 (1988).
[4] C. Guled and B. Singh, Adv. Intell. 137, 577 (2017).
[5] T. Hayat, M. Qasim, and Z. Abbas, Zeitschrift für Naturforschung A **65**, 231 (2010).
[6] A. Borkakoti, and A. Bharali. Q Appl Math. **40**, 461 (1983).
[7] A. Majeed, N. Golsanami, B. Gong, Q. A. Ahmad, S. Rifaqat, A. Zeeshan, and F. M. Noori, Alex. Eng. J. **66**, 543 (2023).
[8] A. Majeed, A. Zeeshan, and M. Jawad, Int. J. Mod. Phys. B, (2022), https://doi.org/10.1142/S0217979223502326
[9] M. Jawad, M. K. Hameed, A. Majeed, and K. S. Nisar, Case Stud. Therm. Eng. **41**, 102574 (2023).
[10] A. Majeed, S. Rifaqat, A. Zeeshan, M. Sh. Alhodaly, and F. M. Noori, Int. J. Mod. Phys. B **37**, 2350088 (2023).
[11] J. F. Collis, Nano Letters (2021).

[12] C. Navier, Royale des Sciences de l'Institut de France. **1**, 414 (1823).
[13] F. T. Akyildiz, Nonlinear Anal. Real World Appl. **12**, 2919 (2011).
[14] C. Wang, Phys. Fluids. **27**, 1915 (1984).
[15] S. Saleem, *et al.*, Chin. J. Phys. **55**, 1615 (2017).
[16] N. Khan, *et al.*, J. Sci. Technol. Arts. **21**, 5 (2021).
[17] S. T. Mohyud-Din, M. A. Noor, and A. Waheed, Commun. Korean Math. Soc. **24**, 605 (2009).
[18] A. M. Wazwaz, J. Comput. Appl. Math. **207**, 129 (2007).
[19] J. H. He, Int. J. Non. **5**, 57 (2002).
[20] J. H. He, Int. J. Non. **34**, 699 (1999).